Supporting Information

Vo et al. 10.1073/pnas.1013865108

SI Results

Multiple Regression for MeHg Concentration in Black-Footed Albatross. The residuals for the model of MeHg concentration were normally distributed ($W = 0.960$, $P = 0.493$) and homoscedastic ($\chi^2 = 0.022$, $df = 1$, $P = 0.882$).

MeHg in Russet-Crowned Motmots and Altamira Orioles. MeHg levels in both russet-crowned motmots and Altamira orioles were significantly lower than those found in black-footed albatrosses ($t = -6.365$, $df = 4$, $P = 0.002$ and $t = -6.315$, $df = 4$, $P < 0.001$, respectively). Additionally, no significant relationship was observed between MeHg concentrations and year for either motmots (adjusted $R^2 = -0.206$, $P = 0.613$) (Fig. S3) or orioles (adjusted $R^2 = -0.233$, $P = 0.656$) (Fig. S3).

SI Discussion

Temporal Trend in δ^{15}N. Signatures of δ^{15}N in marbled murrelet (*Brachyramphus marmoratus*) feathers declined significantly, 1.4 ‰, when museum specimens collected 1895 through 1911 were compared to contemporary samples collected 1998 through 2002 (1). The observed trophic level decline in this endangered seabird species occurred after the collapse of the Pacific sardine (*Sardinops sadax*) fisheries.

Temporal Trend in δ^{13}C. The Suess effect occurs because CO_2 released from burning fossil fuels is isotopically depleted in heavy carbon (^{13}C). Through increased human use and dependence on fossil fuels over time, the composition of carbon stable isotopes in the atmosphere has become diluted with more ^{12}C relative to ^{13}C, resulting in declining atmospheric δ^{13}C values. Primary producers incorporate this signal through photosynthesis, and the effect is, thereby, introduced into food webs.

Additionally, global climate change affects marine primary productivity. Phytoplankton δ^{13}C values increase under rapid population growth and decline under reduced productivity (2). Signals of these isotopic trends are likewise recorded in associated food webs.

It follows then that the δ^{13}C data must be corrected for the effects of both anthropogenic CO_2 production and marine primary productivity fluctuations before it may be used to determine the importance of diet and foraging ecology in black-footed albatross MeHg exposure patterns. After a correction (3) was applied for the Suess effect, the δ^{13}C trend reversed, and a significant increase over time resulted (Fig. S1*C*). Unfortunately, stable isotopes data to support a correction for historical shifts in marine primary productivity in the North Pacific are not available. Nevertheless, it is known that Pacific climate variability exhibits an oscillatory course known as the Pacific Decadal Oscillation (PDO) (4, 5). Since 1890, two full PDO cycles have been identified with cool regimens during 1890–1924 and 1947–1976 and warm regimens during 1925–1946 and 1977 to recent years (4). Responses in primary production and phytoplankton biomass differ by region within the Pacific, and a specific regimen shift can induce both an increase in one area and a decline in another (6). However, black-footed albatrosses range and forage all throughout the North Pacific (15°N to 50°N and 130°E to 110°W) (7) and thereby, composite regional differences in productivity. Furthermore, this study's samples span 1880–2002, encompassing the two complete PDO cycles. Therefore, overall mean change in productivity as observed by the composite index of δ^{13}C feather values may be expected to be minimal. Indeed, the δ^{13}C data corrected for the Suess effect do not reflect oscillatory patterns. It is possible that signals of primary productivity shifts do not figure prominently in the black-footed albatross δ^{13}C data, and a correction may not significantly alter the overall δ^{13}C trend.

Therefore, a change in black-footed albatross diet may be most likely responsible for the observed increase in corrected δ^{13}C over time. Benthic consumers in marine coastal environments are ^{13}C-enriched compared with pelagic or planktonic consumers (8). Black-footed albatrosses predominantly feed on either pelagic flying fish eggs (up to 44% of stomach contents during breeding season) (9) or neon flying squid (up to 89.3% of diet during nonbreeding season) (10). However, their stomach contents have also been found to contain about 7% fish, especially Pacific pomfret, as well as 3–5% large crustaceans such as mysids (*Gnathophausia gigas* and *G. ingens*), isopods (*Anuropus branchiatus*), leptostracans (*Nebaliopsis typical*), and shrimp *Notostomus japonicus*—all of which inhabit deep water and benthic environments. Because typical black-footed albatross foraging behavior includes surface seizing, contact dipping, and scavenging within only the upper meters of the ocean (10, 11), many of these fish and these large crustaceans may have been scavenged. Black-footed albatrosses are well-known to scavenge on bait, landings, and discarded offal from fisheries operations (10). It is possible that the diet of these albatrosses has shifted to a higher proportion of scavenged benthopelagic prey over time, concurrent with the expansion of the Pacific fishing industry. This would be consistent with the higher coefficient of variation in both δ^{13}C and δ^{15}N that is found in more recent individuals (Fig. S1).

Correlation Between Black-Footed Albatross MeHg and Upper Fremont Glacier Dataset. Proxies for atmospheric Hg deposition over the past 270 y were derived from total Hg measurements in ice cores of the Upper Fremont Glacier (WY). We applied simple linear regression on data points paired by closest corresponding year to analyze relationships between albatross MeHg and glacier total Hg as well as albatross MeHg and total Hg deposition rates. Neither total Hg ($\log$[black-footed albatross (BFAL) MeHg ng·g^{-1}] $= 4.145 + 0.254 \times \log$[Upper Fremont Glacier (UFG) total Hg ng/L], adjusted $R^2 < 0.001$, $P = 0.329$) nor total Hg deposition rate ($\log$(BFAL MeHg ng·g^{-1}) $= 4.145 + 0.254 \times \log$ (UFG total Hg deposition rate ng/m^2 per y), adjusted $R^2 = 0.034$, $P = 0.202$) significantly correlated with black-footed albatross MeHg from 1880 to 1995.

Influence of Black-Footed Albatross Collection Locality, Breeding Season, Sex, and Museum Origin on MeHg and Stable Isotopes. Collection locality ($F = 0.557$, $df = 6$, $P = 0.758$), breeding season ($t = -1.880$, $df = 20$, $P = 0.075$), sex ($t = 0.754$, $df = 18$, $P = 0.460$), and museum origin ($t = 1.698$, $df = 21$, $P = 0.105$) were not significantly associated with MeHg concentrations in black-footed albatrosses. Similarly, these factors did not affect δ^{15}N (locality: $F = 0.165$, $P = 0.983$; breeding season: $t = -0.152$, $df = 18$, $P = 0.881$; sex: $t = 0.521$, $df = 18$, $P = 0.608$; museum: $t = 0.833$, $df = 21$, $P = 0.414$) or adjusted δ^{13}C (locality: $F = 1.823$, $P = 0.161$; breeding season: $t = -0.466$, $df = 15$, $P = 0.648$; sex: $t = -0.244$, $df = 19$, $P = 0.810$; museum: $t = 2.125$, $df = 10$, $P = 0.059$).

However, two tests were nearly significant: (*i*) breeding season was marginally significant ($t = -1.880$, $df = 20$, $P = 0.075$), wherein higher MeHg levels were recovered during the nonbreeding season, and (*ii*) adjusted δ^{13}C was higher in University of Washington Burke Museum of Natural History and Culture (UWBM) specimens relative to Museum of Comparative Zoology (MCZ) specimens ($t = 1.698$, $df = 21$, $P = 0.105$). Reasons underlying the

former pattern are not straightforward but may include seasonal changes in diet and annual changes in molt timing. During the breeding season, flying fish eggs, other fish, squid, and crustaceans, respectively, comprise 44%, 6%, 32%, and 5% of the volume of black-footed albatross (n = 172) stomach contents (9). During the nonbreeding season, neon flying squid, Pacific pomfret or other fish, and noncephalopod invertebrates, respectively, constitute 89.3%, 7.7%, and 3.0% of the black-footed albatross diet (10). Given the trophic levels of the predominant prey during the nonbreeding season, it may be anticipated that higher MeHg exposure for the albatrosses would occur during this specific season.

Additionally, albatrosses do not breed and molt simultaneously because both processes are energetically demanding; thus, they molt during the nonbreeding season. However, a successful breeding season, an average of 245 d, accords little remaining time in the year to molt. Consequently, albatrosses commonly alternate breeding years, and nonbreeding years, and feather replacement and growth may occur during the months of the former breeding season (12). Feather levels reflect tissue levels during the period of feather growth (13), and after those feathers are fully formed and growth terminates, no additional real-time recording of tissue MeHg levels occurs. Rather, those replacement feathers after the molt and their snapshot of tissue MeHg levels during the molt period are retained through subsequent seasons until the next molt.

Therefore, variation in molt start dates among individuals may have played some role in recording the seasonality in diet and thus, MeHg levels in feathers. It is conceivable that some fraction of the specimens collected during the breeding season were not breeding (i.e., either immature or skipped breeding) but rather, were undergoing molt. This would result in a mixed sample of feathers that did and did not develop during the months of the breeding season and thus, contribute to the nearly significant difference in feather MeHg concentrations. Because of being only nearly significant, however, it is possible that the observed difference in MeHg between reproductive seasons was merely an artifact of intraspecific variation within the population. Further clarification would require analysis of a total of 44 specimens to detect a significant difference with 0.8 power at the 0.05 significance level.

Given the significant correlation between specimen date and adjusted $\delta^{13}C$ (Fig. S1*C*), it may be anticipated that museum of origin would seem to be a nearly significant factor for adjusted $\delta^{13}C$. Further analysis of adjusted $\delta^{13}C$ on a total of 28 specimens would allow detection of a significant difference between museums with 0.8 power at the 0.05 significance level. It is unclear whether this pattern is truly museum-derived vs. ecologically derived and as such, offers grounds for future research. Regardless, adjusted $\delta^{13}C$ was not a significant factor in the multiple regression analyses for MeHg exposure in the black-footed albatrosses. Overall, future research would benefit from rigorous sampling designs that consider not only year but also breeding season, sex, collection locality, and museum of origin.

Abiotic Methylation of IHg in Museum Specimens. Abiotic MeHg formation from external IHg contamination of specimens may be possible if appropriate methyl donors and environmental parameters exist (14). To the best of our knowledge, this process has yet to be studied in museum specimens. The sequential application of $HgCl_2$ and methyl bromide pesticides in museums over historical time (15, 16) may seem conducive to chemical methylation of Hg on the oldest specimens. However, our recovered trend of higher MeHg concentrations in more recent samples suggests that, if abiotic Hg methylation and external MeHg contamination have occurred, the extent to which these mechanisms have operated seems to be minor.

SI Methods

Sample Preparation. In a class 100 clean room and class 100 exhaust hood, the feathers were washed three times in acetone, three times in ultrapure water (Barnestead nanopure water purification system), and one additional time in acetone and were air-dried for 24 h in the clean hood. Each feather, excluding the calamus, was homogenized and stored in sterile I-Chem jars.

Total Hg Measurements. Liquid Hg II was used to establish the calibration curve on the instrument. Instrument level of detection was 0.005 ng Hg, whereas method level of detection was 0.22 $ng{\cdot}g^{-1}$. Instrument accuracy was set as within 10% of the expected Hg concentration in standard reference materials. Average recovery was 95.75% and 104.49% for MESS-3 and DOLT-3, respectively. During the time of feather analyses, hair samples and hair-certified reference material (GBW 07601; National Analysis Center) were run on the same instrument with 90–110% recovery. Multiple standards were used to cover the range of the calibration curve, and Hg recovery of our reference materials, MESS-3 and DOLT-3, strongly correlates with that of the hair reference material, GBW 07601. Low procedural blanks were defined as at least below 10% of the lowest total Hg reading among the samples.

MeHg Measurements. Instrument level of detection was 50 fg MeHg, and method detection limit was 1 $ng{\cdot}g^{-1}$. Recovery of certified reference material (DORM; National Research Council Canada) averaged 101.82%.

Stable Isotope Measurements. Precision of instrument estimates was 1.4% for carbon and 4.3% for nitrogen based on replicates of standard reference materials.

Statistical Analyses. ***Total Hg replicate measurements.*** We compared total Hg concentrations among triplicate measurements of each black-footed albatross feather sample using one-way ANOVA and linear regression on pair-wise combinations of replicates. We found no significant differences between replicates (F = 0.010, df = 2, P = 0.990) and strong correlation between replicates (adjusted R^2 = 0.739, 0.774, and 0.773, $P < 0.001$ for all).

Outliers. Outliers were identified as greater than 1.5 times the interquartile range beyond the first and third quartiles of each dataset (tarsus length, $\delta^{13}C$, $\delta^{15}N$, log-transformed total Hg, log-transformed MeHg, and log-transformed inorganic Hg in black-footed albatrosses, russet-crowned motmots, and Altamira orioles). Three black-footed albatross individuals were found: one with a short tarsus length, a second with a low $\delta^{13}C$ value, and a third with low measurements for both $\delta^{15}N$ and log-transformed total Hg (Dataset S1). These outliers comprised ~2% (1 of 54) and 8% (2 of 25) of the final total Hg and MeHg datasets, respectively, that were incorporated into the regression analyses. Inclusion of the outlier in the total Hg dataset did not alter its corresponding regression results. However, the outliers exhibited disproportionate influence in the multiple regression analysis for MeHg, and their inclusion resulted in a different model chosen (corrected $\delta^{13}C$ + δ15N) to best explain the variation in observed MeHg levels among the black-footed albatross samples [n = 25, K = 2, adjusted R^2 = 0.442, P = 0.001, Akaike's information criterion (AIC_c) = 5.69, ΔAIC = −2.51, w_i = 0.64]. Outliers were excluded to render the data more representative of the study population and enhance the accuracy of estimates from the regressions. Removal of outliers before statistical analyses significantly reduces errors of inference in most cases and generally comprises established precedence (17).

Motmot and oriole dataset. We hypothesized that exposure in russet-crowned motmots and Altamira orioles during the time period sampled should only reflect museum contamination and should not differ between species. Therefore, mean total Hg concentrations

were compared by a paired t test on russet-crowned motmot and Altamira oriole individuals, and we found no significant difference in mean IHg exposure between species among samples paired by decade ($t = 0.658$, $df = 6$, $P = 0.534$). Therefore, we applied simple linear regression to the combined motmot and oriole dataset to analyze the relationship between IHg and year.

Model determination. We arrived at the most parsimonious model by starting with the global model, which included all predictor variables, and subsequently removing nonsignificant terms in step-wise fashion. We used residual sum of squares to determine the relative significance of relationships between feather MeHg levels and the a priori predictor variables. The model selection process was carried out as long as the residual sum of squares was not significantly increased because of term removal until all nonsignificant terms were removed. On the removal of each nonsignificant term, we added any outliers that had been previously excluded from the analysis because of the term in the analysis. A correlation matrix revealed a lack of covariance between terms ($r < 0.65$). All terms containing interactions between predictors were found to be nonsignificant. To simplify presentation of the results, these interaction terms were not included in the global model.

$\delta^{13}C$ correction. The equation $-(-4{,}577.8 + 7.3430\,t - 3.9213 \times 10^{-3}t^2 + 6.9812 \times 10^{-7}t^3)$ modeled atmospheric $\delta^{13}C$ ($\delta^{13}C_{atm}$) for any given year t, and the change in modeled $\delta^{13}C_{atm}$ over time was because of anthropogenic fossil fuel burning. The year 1880, the earliest sample date, served as the reference year, and the decline in modeled $\delta^{13}C_{atm}$ between 1880 and sample year t was added back to the measured $\delta^{13}C$ of the sample to obtain a corrected value.

Model evaluation. We used AIC corrected for small sample size (AIC_c) and evaluated the relative importance of the models by normalizing their likelihoods [$L(\theta)$] to positive Akaike's weights (w_i) where (i) $AIC_c = -2\log[L(\theta)] + 2K + [2K(K+1)/(n-K-1)]$, with sample size n and K parameters, (ii) $\Delta_i = AIC_c - AIC_{min}$, and ($iii$) $w_i = [\exp(-0.5\ \Delta_i)]/\Sigma[\exp(-0.5\ \Delta_r)]$, with model number i or r and summation (Σ) of $\exp(-0.5\ \Delta_r)$ from r equals one to R total number of models (18).

Tests for regression assumptions. The Shapiro–Wilk Test and nonconstant variance test were used to check normality and homoscedasticity of error terms, respectively, in the regression analyses.

Evaluation of Sampling Methods. Although high within-individual variation in total Hg concentrations has been reported (19) for Arctic terns (*Sterna paradisaea*), common terns (*Sterna hirundo*), and Leach's storm petrels (*Oceanodroma leucorhoa*), a paired t test on left and right breast feathers of five black-footed albatross individuals indicated no significant difference in mean total Hg sequestration between sides of the breast ($t = -0.449$, $df = 25$, $P = 0.658$). However, large within-feather variation in total Hg measurements was observed. The range relative to mean of replicate measurements per feather varied from 5.61% to 86.04%. Nevertheless, there were no significant differences in mean total Hg measurements between replicate groups ($F_{2,159} = 0.001$, $P = 0.990$), and there were significantly good pair-wise correlations between replicate measurements (lowest adjusted $R^2 = 0.739$, $P < 0.001$). Similarly, replicate measurements on a subset ($n = 7$) of all black-footed albatross feather samples that underwent MeHg analyses ($n = 25$) exhibited high within-feather variation in range relative to mean of replicates (inorganic Hg: 3.17–189.5%; MeHg: 0.96–17.89%). Despite this variation, comparison of mean measurement values between replicates using a paired t test revealed no significant differences (inorganic Hg: $t = -1.130$, $df = 6$, $P = 0.301$; MeHg: $t = 0.875$, $df = 6$, $P = 0.415$), and replicate measurements were significantly correlated (inorganic Hg: adjusted $R^2 = 0.866$, $P = 0.00147$; MeHg: adjusted $R^2 = 0.911$, $P < 0.001$).

Therefore, for total Hg data, replicate measurements were averaged to represent each sample. For MeHg and IHg data, replicate values were not included in statistical procedures, because only a subset of samples was rerun among all black-footed albatross samples from the MeHg analyses. We speculate that the high within-feather variation encountered in this study may be because of low sample masses analyzed or high variation in Hg sequestration within different parts of each feather (i.e., rachis, barbs, and barbules). Because the feathers contained such high Hg levels, low sample masses were necessary to remain within the standardized calibrations of the analytical instruments. Furthermore, it is known that Hg is differentially distributed among distal and proximal locations within a feather (20). Although each feather was homogenized as much as possible, differential composition of subsamples used to obtain measurements combined with error related to the analysis of low sample masses may have lead to the wide ranges in observed total Hg measurements.

1. Becker BH, Beissinger SR (2007) Centennial decline in the trophic level of an endangered seabird after fisheries decline. *Conserv Biol* 20:470–479.
2. Laws EA, Popp BN, Bidigare RR, Kennicutt MC, Macko SA (1995) Dependence of phytoplankton carbon isotopic composition on growth rate and [CO2] (aq): Theoretical considerations and experimental results. *Geochim Cosmochim Ac* 59: 1131–1138.
3. Schelske CL, Hodell DA (1995) Using carbon stable isotopes of bulk sedimentary organic matter to reconstruct the history of nutrient loading and eutrophication in Lake Erie. *Limnol Oceanogr* 40:918–929.
4. Biondi F, Gershunov A, Cayan DR (2001) North Pacific decadal climate variability since 1661. *J Climate* 14:5–10.
5. Mantua NJ, Hare SR (2002) The Pacific decadal oscillation. *J Oceanogr* 58:35–44.
6. Aita MN, Yamanaka Y, Kishi MJ (2007) Interdecadal variation of the lower trophic ecosystem in the northern Pacific between 1948 and 2002, in a 3-D implementation of the NEMURO model. *Ecol Model* 202:81–94.
7. Lewison RL, Crowder LB (2003) Estimating fishery bycatch and effects on a vulnerable seabird population. *Ecol Appl* 13:743–753.
8. France RL (1995) Differentiation between littoral and pelagic food webs in lakes using stable carbon isotopes. *Limnol Oceanogr* 40:1310–1313.
9. Harrison CS, Hida TS, Seki MP (1983) Hawaiian seabird feeding ecology. *Wildl Monogr* 85:3–71.
10. Gould P, Ostrom P, Walker W (1997) Trophic relationships of albatrosses associated with squid and large-mesh drift-net fisheries in the north Pacific Ocean. *Can J Zoolog* 75:549–562.
11. Miller L (1940) Observations on the black-footed albatross. *Condor* XLII:229–238.
12. Langston NE, Rohwer S (1996) Molt-breeding tradeoffs in albatrosses: Life history implications for big birds. *Oikos* 76:498–510.
13. Furness RW, Muirhead SJ, Woodburn M (1986) Using bird feathers to measure mercury in the environment: Relationships between mercury content and moult. *Mar Pollut Bull* 17:27–30.
14. Celo V, Lean DR, Scott SL (2006) Abiotic methylation of mercury in the aquatic environment. *Sci Total Environ* 368:126–137.
15. Sirois PJ, Sansoucy G (2001) Analysis of museum objects for hazardous pesticide residues: A guide to techniques. *Collection Forum* 17:49–66.
16. Ornstein L (2010) Poisonous Heritage: Pesticides in Museum Collections. Masters Thesis (Seton Hall University, South Orange, NJ).
17. Barnett V, Lewis T (1994) *Outliers in Statistical Data* (Wiley, New York).
18. Burnham KP, Anderson DR (2002) *Model Selection and Multimodel Inference: A Practical Information-Theoretic Approach* (Springer, New York).
19. Bond AL, Diamond AW (2008) High within-individual variation in total mercury concentration in seabird feathers. *Environ Toxicol Chem* 27:2375–2377.
20. Berg W, Johnels A, Sjöstrand B, Westermark T (1966) Mercury content in feathers of Swedish birds from the past 100 years. *Oikos* 17:71–83.

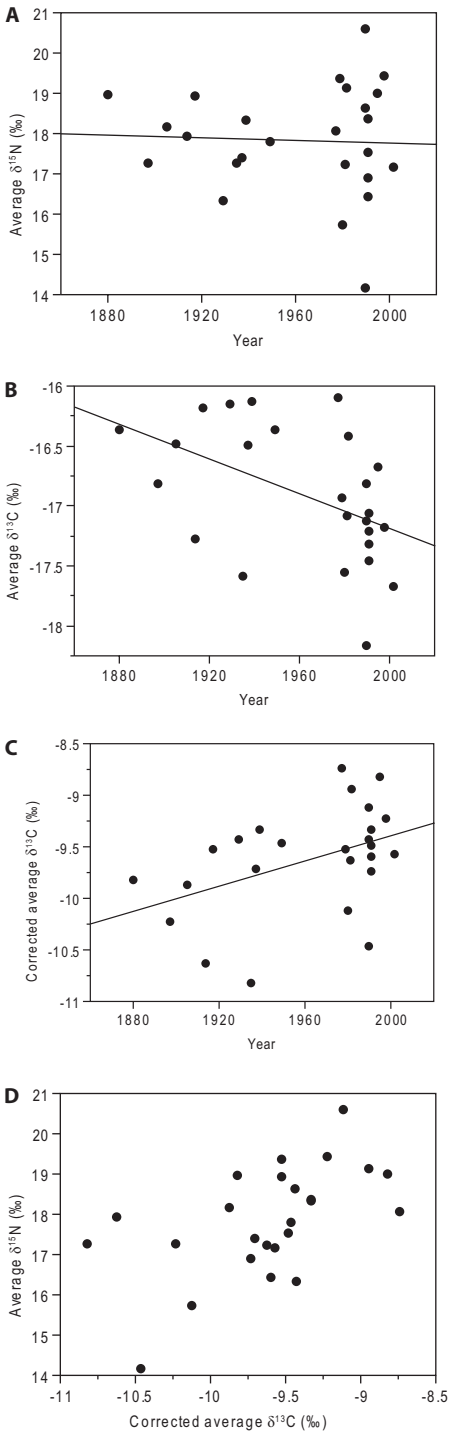

Fig. S1. Temporal trends in carbon and nitrogen stable isotopes in the breast feathers of black-footed albatross museum specimens (n = 22) collected from 1880 to 2002 from across the north Pacific Ocean. (*A*) Average $\delta^{15}N = 19.362 - 0.001 \times$ year, adjusted $R^2 = -0.050$, and $P = 0.924$. (*B*) Average $\delta^{13}C = -4.075 - 0.007 \times$ year, adjusted $R^2 = 0.228$, and $P = 0.014$. (*C*) Suess effect-corrected average $\delta^{13}C = -31.261 + 0.008 \times$ year, adjusted $R^2 = 0.357$, and $P = 0.002$. (*D*) Scatter plot of average $\delta^{15}N$ and corrected average $\delta^{13}C$.

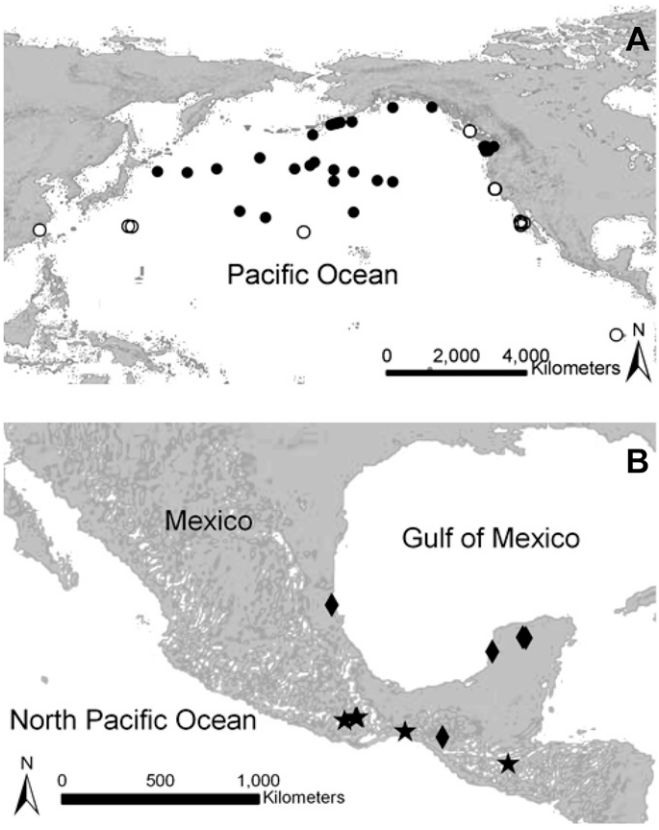

Fig. S2. Collection localities of (*A*) black-footed albatross museum specimens from the Harvard University Museum of Comparative Zoology (open circles; collected 1880–1949, $n = 23$) and University of Washington Burke Museum of Natural History and Culture (closed circles; collected 1917–2002, $n = 31$) analyzed for total mercury (n = all 54 samples), methylmercury ($n = 25$ of 54 available samples), and inorganic mercury ($n = 25$ of 54 available samples). (*B*) Russet-crowned motmot (stars; collected 1890–2004, $n = 5$) and Altamira oriole (diamonds; collected 1865–1995, $n = 5$) specimens from five different museums in the United States analyzed for methylmercury and inorganic mercury.

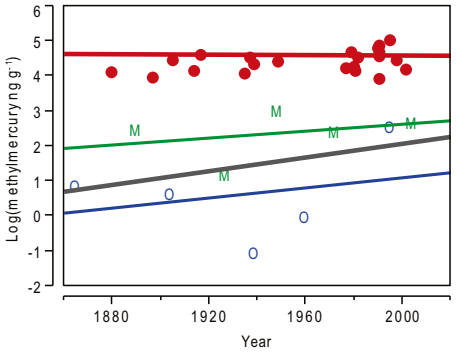

Fig. S3. Temporal trends in methylmercury concentrations in the breast feathers of black-footed albatross ($n = 23$), russet-crowned motmot ($n = 5$), and Altamira oriole ($n = 5$) museum specimens spanning 1865–2004. Red line is albatross: log(methylmercury ng·g^{-1}) = −2.113 + 0.003 × year, adjusted $R^2 = 0.133$, and $P = 0.0489$. Fig. 1 has more details. Green line is motmot: log(methylmercury ng·g^{-1}) = −7.252 + 0.005 × year, adjusted $R^2 = -0.206$, and $P = 0.613$. Blue line is oriole: log(methylmercury ng·g^{-1}) = −13.343 + 0.007 × year, adjusted $R^2 = -0.233$, and $P = 0.656$. Gray line is motmot and oriole combined: log(methylmercury ng·g^{-1}) = −21.182 + 0.012 × year, adjusted $R^2 = 0.058$, and $P = 0.262$.

Table S1. Trends in historical and recent anthropogenic mercury emissions as measured through deposition or exposure levels of various abiotic and biotic matrices from the Pacific region and worldwide

Matrix	Record	Location	Time frame	Measured	Method	Trend direction	Concentration range*	Flux range†	Average flux ratio	Ref.
Pacific region										
Lake sediment	Atmospheric deposition	Alaskan Arctic	50–2000	Total Hg	CVAFS	↑C and ↑F until 1990	32–186 $ng \cdot g^{-1}$	2–20 $\mu g \cdot m^{-2}$ per y^{-1}	2.5-fold (1840–2000)	1
Bay sediments	Atmospheric deposition	Liaodong Bay, China	1890–2000	Total Hg	IC-PMS	↑C and ↑F after late 1970s	0.024–0.24 $mg \cdot kg^{-1}$‡	0.01–0.075 $\mu g \cdot m^{-2}$ per y^{-1}	—	2
Estuary sediments	Atmospheric deposition	Pear River Estuary, China	1835–2000	Total Hg	FIMS	↑C and ↑F during most recent three decades	112.5–212.5 $ng \cdot g^{-1}$	400–3200 $ng \cdot cm^{-2}$ per $decade^{-1}$	9-fold (1900–1990) and 3-fold (1950–1990)	3
Over ocean gas	Atmospheric deposition	Pacific Ocean, Northern Hemisphere	1980–2004	Total gaseous Hg		Insufficient data to evaluate significance of recent ↑C	1.5–2.5 $ng \cdot m^{-3}$	—	—	4
Marine water	Atmospheric deposition	Pacific Ocean, Northern Hemisphere	1987, 2002, and 2006	Total dissolved gaseous Hg		Similar C between 1987 and 2002, higher C in 2006	0.03–4.43 pmol	0.03–230 $ng \cdot m^{-2}$ per d^{-1}	—	4–6
Lake sediment	Atmospheric deposition	Fraser River Basin, British Columbia	<1900–1994	Total Hg	DMA	Singular peak 1940–1960	12.5–158 $ng \cdot g^{-1}$	10 $kg \cdot y^{-1}$	1.7- to 8.1-fold (1870–1990)	7
Global										
Ice	Atmospheric deposition	Upper Fremont Glacier, Wyoming	1720–1993	Total Hg	CVAFS	↑C and ↑F over time, precipitous ↑ 1950–1990, ↓ in early 1990s, specific peaks during 1850–1884, 1940–1945, and 1980	1.21–34.97 $ng \cdot L^{-3}$	416–29,736 $ng \cdot cm^{-2}$ per y^{-1}	20-fold	8
Ice	Atmospheric deposition	Greenland	1940–2006	Gaseous elemental Hg	Gas-phase mercury analyzer	↑ to max in 1970, stabilization ~1995	1.5–3 $ng \cdot m^{-3}$§	—	—	9
Ice	Atmospheric deposition	Blukha Mountain, Russia	1925–2001	Reactive and total Hg	CVAFS	↑C over time	0.2–6.3 $ng \cdot kg^{-1}$	—	—	10
Soil	Atmospheric deposition	Hokkaido, Japan	31996 BC to 2004 AD	Total Hg	DMA	↑F over geological ages post-1600 y BP (2004)	1–173 $\mu g \cdot kg^{-1}$	2.1–14.1 $\mu g \cdot m^{-2}$ per y^{-1}	—	11
Lake sediment	Atmospheric deposition	Nova Scotia	1000–1997	Total Hg		↑C and ↑F over time, especially after industrial revolution	20–120 $ng \cdot g^{-1}$	1–19 $\mu g \cdot m^{-2}$ per y^{-1}	5-fold	12
Lake sediment	Atmospheric deposition	New Zealand	1200–1997	Total Hg		↑C and ↑F over time, especially after industrial revolution	40–280 $ng \cdot g^{-1}$	2–48 $\mu g \cdot m^{-2}$ per y^{-1}	3-fold	12
Lake sediment	Atmospheric deposition	Central and Northern Canada	1829–1994	Total Hg	FAS	↑C and ↑F over time	15.8–159 $ng \cdot g^{-1}$	1.1–114 $\mu g \cdot m^{-2}$ per y^{-1}	—	13
Lake sediment	Atmospheric deposition	Arctic	1750–1993	Total Hg	CVAFS	↑C and ↑F over time	30–159 ng g^{-1}	0.2–1.8 $ng \cdot cm^{-2}$ per y^{-1}	2-fold (1750–1867), 3-fold (1867–1990), and 6-fold (1750–1980)	14
Lake sediment	Atmospheric deposition	Minnesota and Wisconsin	1700–1990	Total Hg	CVAFS	↑C and ↑F over time	—	3–12.5 $\mu g \cdot m^{-2}$ per y^{-1}	3.7-fold	15

Table S1. Cont.

Matrix	Record	Location	Time frame	Measured	Method	Trend direction	Concentration range*	Flux range†	Average flux ratio	Ref.
Lake sediment	Atmospheric deposition	Nevada	1450–2000	Total Hg	CVAFS	↑C and ↑F over time, dramatic 1920–1980	0.033–0.191 ppm¶	2.0–47 $\mu g \cdot m^{-2}$ per y^{-1}	24-fold	16
Lake sediment	Atmospheric deposition	National Parks, Western United States	1775–2003	Total Hg	CVAFS	↑C and ↑F over time	84–288 $ng \cdot g^{-1}$	3.1–11.7 $\mu g \cdot m^{-2}$ per y^{-1}	3.2-fold	17
Lake sediment	Atmospheric deposition	Adirondack Lakes	1780–1983	Total Hg	FAS	↑C and ↑F since 1850	0.08–0.50 $\mu g \cdot g^{-1}$	5.0–8.9 $\mu g \cdot m^{-2}$ per y^{-1}	3.5-fold	18
Lake sediment	Atmospheric deposition	Vermont and New Hampshire	1800–1998	Total Hg	CVAFS	↑C and ↑F over time, peaks in 1950 or later and ↓ in recent decades	0.06–0.66 $\mu g \cdot g^{-1}$	5–83 $\mu g \cdot m^{-2}$ per y^{-1}	3.9-fold	19
Lake sediment	Atmospheric deposition	New England	1875–1998	Total Hg	CVAFS	↑F from end of 18th century to max 1970–1990	100–250 $ng \cdot g^{-1}$	0–50 $\mu g \cdot m^{-2}$ per y^{-1}	1- to 3-fold	20
Lake sediment	Atmospheric deposition	Greenland	350–2000	Total Hg	CVAFS	↑F starting mid-1800s to 1970s/1980s with subsequent ↓	6–440 $ng \cdot g^{-1}$‖	1–10 $\mu g \cdot m^{-2}$ per y^{-1}	2- to 3-fold	21
Lake sediment	Atmospheric deposition	Sweden	<2890 BC to 1998 AD	Total Hg	CVAFS	↑C post-1850	30–880 $ng \cdot g^{-1}$**	—	—	22
Lake sediment	Atmospheric deposition	Patagonia	1200–2009	Total Hg		Abrupt ↑C and ↑F over time	50–500 ng g^{-1}	15–150 $\mu g \cdot m^{-2}$ per y^{-1}	—	23
Seal hair	Bioaccumulation	Antarctica	2–2002	Total Hg		Peaks in C during five episodes of extensive global gold/silver mining activities	890–1740 $ng \cdot g^{-1}$	—	—	24
Coral	Bioaccumulation	Venezuela	1900–1999	Total Hg	AFS	↑C and ↑F over time	—	—	—	25

CVAFS, cold vapor atomic fluorescence spectrometry; C, Hg concentration; F, Hg flux or deposition rate; FIMS, flow injection mercury system; IC-PMS, inductively coupled plasma mass spectrometry.

*Units of concentrations reported in the literature vary: $ng \cdot g^{-1}$, $mg \cdot kg^{-1}$, $ng \cdot m^{-3}$, pmol, $ng \cdot L^{-3}$, $ng \cdot kg^{-1}$, $\mu g \cdot kg^{-1}$, ppm, and $\mu g \cdot g^{-1}$.

†Units of fluxes reported in the literature vary: $\mu g \cdot m^{-2}$ per y^{-1}, $ng \cdot cm^{-2}$ per $decade^{-1}$, $ng \cdot m^{-2}$ per d^{-1}, $kg \cdot y^{-1}$, and $ng \cdot cm^{-2}$ per y^{-1}.

‡Average enrichment factor: 1- (1890–1950) and 10-fold (1970–2000).

§Average enrichment factor: 2-fold (1940–1970s).

¶Average enrichment factor: 4.9-fold.

‖Average enrichment factor: 3-fold.

**Average enrichment factor: 3.9-fold.

1. Fitzgerald WF, et al. (2005) Modern and historic atmospheric mercury fluxes in northern Alaska: Global sources and Arctic depletion. *Environ Sci Technol* 39:557–568.
2. Xu B, et al. (2009) The trend and extent of heavy metal accumulation over last one hundred years in the Liaodong Bay, China. *Chemosphere* 75:442–446.
3. Shi J, Ip CC, Zhang G, Jiang GB, Li XD (2010) Mercury profiles in sediments of the Pearl River Estuary and the surrounding coastal area of South China. *Environ Pollut* 158:1974–1979.
4. Sprovieri F, Pirrone N, Mason RP, Andersson M (2009) in *Mercury Fate and Transport in the Global Atmosphere*, eds, Pirrone N, Mason R (Springer, New York), pp 323–380.
5. Laurier FJG, Mason RP, Gill GA, Whalin L (2004) Mercury distributions in the North Pacific Ocean—20 years of observations. *Mar Chem* 90:3–19.
6. Sunderland EM, Krabbenhoft DP, Moreau JW, Strode SA, Landing WM (2009) Mercury sources, distribution, and bioavailability in the North Pacific Ocean: Insights from data and models. *Global Biogeochem Cy* 23:1–14.
7. Gallagher L, Macdonald RW, Paton DW (2004) The historical record of metals in sediments from six lakes in the Fraser River Basin, British Columbia. *Water Air Soil Poll* 152:257–278.
8. Schuster PF, et al. (2002) Atmospheric mercury deposition during the last 270 years: A glacial ice core record of natural and anthropogenic sources. *Environ Sci Technol* 36:2303–2310.
9. Faïn X, et al. (2009) Polar firn air reveals large-scale impact of anthropogenic mercury emissions during the 1970s. *Proc Natl Acad Sci USA* 106:16114–16119.
10. Frolova NS, Eyrikh SS, Papina TS, Schwikowski M (2008) Time-space estimate of the variation in a level of mercury pollution of the altai atmosphere according to layer-by-layer analysis of high mountain glacier core of Belukha Mountain. *Chemistry for Sustainable Development* 16:227–234.
11. Hobara S, Mizuno N, Amano Y, Yokota H, Taniyama H (2009) Mercury distribution in tephra soil layers in Hokkaido, Japan, with reference to 34,000-year stratification. *Soil Sci Plant Nutr* 55:582–589.
12. Lamborg CH, et al. (2002) Modern and historic atmospheric mercury fluxes in both hemispheres: Global and regional mercury cycling implications. *Global Biogeochem Cy* 16: 1104–1114.
13. Lockhart WL, et al. (1998) Fluxes of mercury to lake sediments in central and northern Canada inferred from dated sediment cores. *Biogeochemistry* 40:163–173.
14. Hermanson MH (1998) Anthropogenic mercury deposition to arctic lake sediments. *Water Air Soil Pollut* 101:309–321.
15. Swain EB, Engstrom DR, Brigham ME, Henning TA, Brezonik PL (1992) Increasing rates of atmospheric mercury deposition in midcontinental North America. *Science* 257:784–787.
16. Heyvaert AC, Reuter JE, Slotton DG, Goldman CR (2000) Paleolimnological reconstruction of historical atmospheric lead and mercury deposition at Lake Tahoe, California–Nevada. *Environ Sci Technol* 34:3588–3597.
17. Mast MA, Manthorne DJ, Roth DA (2010) Historical deposition of mercury and selected trace elements to high-elevation national parks in the western US inferred from lake-sediment cores. *Atmos Environ* 44:2577–2586.
18. Lorey P, Driscoll CT (1999) Historical trends of mercury deposition in Adirondack lakes. *Environ Sci Technol* 33:718–722.
19. Kamman NC, Engstrom DR (2002) Historical and present fluxes of mercury to Vermont and New Hampshire lakes inferred from 210Pb dated sediment cores. *Atmos Environ* 36: 1599–1609.
20. Perry E, Norton SA, Kamman NC, Lorey PM, Driscoll CT (2005) Deconstruction of historic mercury accumulation in lake sediments, northeastern United States. *Ecotoxicology* 14:85–99.
21. Bindler R, Renberg I, Appleby PG, Anderson NJ, Rose NL (2001) Mercury accumulation rates and spatial patterns in lake sediments from west Greenland: A coast to ice margin transect. *Environ Sci Technol* 35:1736–1741.
22. Bindler R, Olofsson C, Renberg I, Frech W (2001) Temporal trends in mercury accumulation in lake sediments in Sweden. *Water Air Soil Poll* 1:343–355.
23. Guevara SR, Meili M, Rizzo A, Daga R, Arribére M (2010) Sediment records of highly variable mercury inputs to mountain lakes in Patagonia during the past millennium. *Atmos Chem Phys* Discuss 9:25885–25914.
24. Sun L, et al. (2006) A 2000-year record of mercury and ancient civilizations in seal hairs from King George Island, West Antarctica. *Sci Total Environ* 368:236–247.
25. Ramos R, Cipriani R, Guzman HM, García E (2009) Chronology of mercury enrichment factors in reef corals from western Venezuela. *Mar Pollut Bull* 58:222–229.

Dataset S1. Raw data collected from breast feathers of black-footed albatross (*n* = 54), russet-crown motmot (*n* = 5), and Altamira oriole (*n* = 5) museum specimens analyzed for total mercury, methylmercury, inorganic mercury, and/or carbon and nitrogen stable isotopes

Dataset S1 (XLS)

MCZ, Harvard Museum of Comparative Zoology; UWBM, the University of Washington Burke Museum; MVZ, the University of California Berkeley Museum of Vertebrate Zoology; AMNH, American Museum of Natural History; WFVZ, Western Foundation of Vertebrate Zoology; UNLV, University of Nevada, Las Vegas Marjorie Barrick Museum; HSPH, the Harvard School of Public Health Trace Metals Analysis Laboratory; Dartmouth, the Dartmouth College Trace Metals Analytical Laboratory; U, unknown; n/a, not analyzed. Italicized black-footed albatross individuals were identified as outliers and excluded from analyses: one in each of the tarsus length and $\delta^{13}C$ datasets and a third in both the $\delta^{15}N$ and log-transformed total Hg datasets.